Superconducting properties of the attractive Hubbard model in the slave-boson approach

1998 J. Phys.: Condens. Matter 10 9029

(http://iopscience.iop.org/0953-8984/10/40/009)

J. Phys.: Condens. Matter **10** (1998) 9029–9054. Printed in the UK PII: S0953-8984(98)94846-9

Superconducting properties of the attractive Hubbard model in the slave-boson approach

M Bąk† and R Micnas‡

Institute of Physics, A Mickiewicz University, Umultowska 85, PL-61-614 Poznań, Poland

Received 4 June 1998, in final form 31 July 1998

Abstract. The attractive Hubbard model for normal and superconducting ground states is examined for arbitrary electron concentration by the use of the slave-boson mean-field approximation (SBMFA) technique. This approach, at a saddle-point level, is equivalent to the Gutzwiller approximation. Several superfluid characteristics of the model are shown for hypercubic lattices of all dimensions, including $d = \infty$, and a comparison with the Bardeen–Cooper–Schrieffer Hartree–Fock approximation (BCS-HFA) calculations and exact results is made. Our results show quantitative and qualitative corrections of the SBMFA to the HFA. The improvement of the SBMFA over the HFA diminishes with increasing lattice dimensionality. We have also evaluated the energy difference between the superconducting and the normal states; this is compared with available results for the superconducting critical temperatures in various dimensions and Uemura-type plots are obtained. The results confirm and substantiate the assertion of a continuous evolution of the superfluid properties of the model from the weak-coupling (BCS-like) to the strong-coupling (composite-boson superconductivity) limit.

1. Introduction

The Hubbard model is widely employed in problems concerning metal–insulator transitions, ferromagnetism, superconductivity and high-temperature superconductivity. Despite its formal simplicity, it has been solved exactly only for one dimension [1], while for higher dimensions only approximate solutions have been obtained. Much effort has been devoted to the $d = 2$ case, which is related to high-temperature superconductors (HTS).

The local electron pairing and strong correlations are best described by the negative-U extended Hubbard model, in which the on-site local attraction can result from the coupling of narrow-band electrons to a bosonic field (phonons, excitons etc), upon elimination of bosonic degrees of freedom, or from electronic mechanisms (for a review, see [2]). Such a model has been considered as the effective model of extreme type II superconductors with s-wave pairing including the doped barium bismuthates, fullerides and Chevrel phases. It can also lead to some relevant understanding in the field of cuprate HTS [2–4].

The description of the superconducting state of the attractive Hubbard model is good only in the limits of weak and strong coupling. For intermediate values of the interaction, both the Hartree–Fock approximation (HFA) and the strong-coupling expansions are less reliable. The purpose of this paper is to examine the properties of the model for hypercubic lattices for one, two, three and an infinite number of dimensions in the slave-boson approach. The slave-boson method improves on the HFA results, because it takes into account the

† E-mail: karen@delta.amu.edu.pl.
‡ E-mail: rom@alpha.amu.edu.pl.

0953-8984/98/409029+26$19.50

on-site electron correlations. It is not restricted to strong- or weak-coupling limits and it can also give credible results for the intermediate-coupling regime. In the saddle-point approximation this approach is equivalent to the Gutzwiller approximation of the Gutzwiller wave function; however, it enables us to go beyond that approximation [5]. We use this method at a saddle-point level to investigate the behaviour of the Hubbard model, including its electromagnetic properties, for different, realistic densities of states and to examine the applicability of the infinite-dimension limit [6] as an approximation to the three-dimensional case in this type of calculation. We evaluate the properties of the negative-U Hubbard model with arbitrary electron filling (which is equivalent to the positive-U Hubbard model at half-filling in an effective magnetic field) and in particular we analyse the crossover from BCS-like superconductivity, with extended Cooper pairs, to superconductivity of composite bosons (local Cooper pairs), which occurs when one passes from a weak- to a strong-coupling regime (from $|U| \ll t$ to $|U| \gg t$) [2–4].

This is particularly relevant for HTS, which, having a short coherence length comparable to the average interparticle spacing, fall into the intermediate region between BCS physics and the preformed electron pair scenario [7, 8].

Related studies were performed for $d = 2$ at half-filling by Denteneer [9] and for a square density of states by Sofo and Balseiro [10] as well as by Bułka and Robaszkiewicz [11].

The paper is organized as follows. In section 2 we outline the slave-boson method and present the free energies in the superconducting and normal phases as well as the formulae for the electromagnetic properties. Section 3 presents our results for the superconducting and electromagnetic properties of the model for various lattices versus the coupling strength and the electron filling. These results are compared with the exact solution for $d = 1$, those from the Bardeen–Cooper–Schrieffer HFA approach and those from other treatments. We also discuss the scaling properties of the model, including the variations of the condensation energy, the superfluid density and the ratio of the energy gap to the critical temperature, as well as the infinite-dimensional case. We conclude the work in section 4. The appendix contains an alternative derivation of the main equations used in the SBMFA (slave-boson mean-field approximation) method without resorting to the electron–hole transformation.

2. The slave-boson approach

In this section we describe the slave-boson method and apply it to the negative-U Hubbard model. In the standard notation the model takes the form

$$H = -t \sum_{i,j,\sigma} c_{i\sigma}^{\dagger} c_{j\sigma} - U \sum_{i} n_{i\uparrow} n_{i\downarrow} - \mu \sum_{i,\sigma} n_{i\sigma} \tag{1}$$

and the number of electrons per lattice site is given by

$$n = N_e/N = (1/N) \sum_{i\sigma} \langle n_{i\sigma} \rangle.$$

From several possible ways of introducing slave bosons, we have chosen that adopted by Kotliar and Ruckenstein [5]. This consists in connecting an auxiliary boson with each of four possible electronic states (on every lattice site): $|0\rangle$, $|\sigma\rangle$, $|2\rangle$ and assuming that they are created out of the new vacuum state. These are

$$|0\rangle = e^{\dagger}|v\rangle \qquad |\sigma\rangle = p_{\sigma}^{\dagger} f_{\sigma}^{\dagger}|v\rangle \qquad |2\rangle = d^{\dagger} f_{\uparrow}^{\dagger} f_{\downarrow}^{\dagger}|v\rangle \tag{2}$$

where the f_{σ} fulfil the fermion commutation relations and e, p_{σ}, d fulfil the boson commutation relations. There are two constraints imposed on the system:

$$f_{i\sigma}^{\dagger} f_{i\sigma} = p_{i\sigma}^{\dagger} p_{i\sigma} + d_i^{\dagger} d_i \qquad \sum_{\sigma} p_{i\sigma}^{\dagger} p_{i\sigma} + e_i^{\dagger} e_i + d_i^{\dagger} d_i = 1. \tag{3}$$

The electron annihilation operator can be expressed as

$$c_{i\sigma} = (e_i^\dagger p_{i\sigma} + p_{i\bar{\sigma}}^\dagger d_i) f_{i\sigma}. \tag{4}$$

Through the electron–hole transformation, the attractive Hubbard model on a bipartite lattice for arbitrary band filling (with the additional pairing field $\lambda^{(0)}$) is transformed into the repulsive one at half-filling, in the magnetic field $h = 2\mu + U$ and with fixed magnetization $m_z = n - 1$. The superconducting order parameter

$$2x_0 = \langle c_{i\uparrow}^\dagger c_{i\downarrow}^\dagger \rangle + \langle c_{i\downarrow} c_{i\uparrow} \rangle$$

is transformed into staggered magnetic ordering in the x–y plane:

$$m_x = \langle c_{i\uparrow}^\dagger c_{i\downarrow} + c_{i\downarrow}^\dagger c_{i\uparrow} \rangle \exp(\mathrm{i}\boldsymbol{Q} \cdot \boldsymbol{R}_i)$$

where $\boldsymbol{Q} = (\pi/a, \pi/a, \pi/a, \ldots)$ is a half of the smallest reciprocal-lattice vector, and the charge operators transform into the spin operators and vice versa [2]. One then obtains

$$\begin{aligned} H = -t \sum_{i,j,\sigma} c_{i\sigma}^\dagger c_{j\sigma} + U \sum_i n_{i\uparrow} n_{i\downarrow} - \frac{U}{2} \sum_{i\sigma} n_{i\sigma} - \frac{h}{2} \sum_i (n_{i\uparrow} - n_{i\downarrow}) \\ - \frac{\lambda^{(0)}}{2} \sum_i \left(\eta_i (c_{i\uparrow}^\dagger c_{i\downarrow} + c_{i\downarrow}^\dagger c_{i\uparrow}) - m_x \right) \end{aligned} \tag{5}$$

where $\eta_i = \exp(\mathrm{i}\boldsymbol{Q} \cdot \boldsymbol{R}_i)$. Next, we follow the procedure of Sofo and Balseiro [10], and apply the canonical transformation consisting in rotation of the spin operators to a new quantization axis aligned with the induced magnetization. Only now do we introduce the slave-boson operators and perform mean-field factorization. The final effect of the above analysis is linearization of the Hamiltonian, at the expense of the appearance of the band-narrowing factor in the hopping term.

The canonical transformation of the electron operators is of the form

$$\begin{pmatrix} c_{i\uparrow} \\ c_{i\downarrow} \end{pmatrix} = \begin{pmatrix} \cos\phi_i & -\sin\phi_i \\ \sin\phi_i & \cos\phi_i \end{pmatrix} \begin{pmatrix} c'_{i\uparrow} \\ c'_{i\downarrow} \end{pmatrix} \tag{6}$$

which corresponds to the rotation of the spin operators:

$$\begin{pmatrix} S_{ix} \\ S_{iy} \\ S_{iz} \end{pmatrix} = \begin{pmatrix} \cos\theta_i & 0 & \sin\theta_i \\ 0 & 1 & 0 \\ -\sin\theta_i & 0 & \cos\theta_i \end{pmatrix} \begin{pmatrix} S'_{ix} \\ S'_{iy} \\ S'_{iz} \end{pmatrix} \tag{7}$$

where

$$\begin{aligned} &S_{ix} = (S_i^\dagger + S_i^-)/2 \qquad S_{iy} = (S_i^\dagger - S_i^-)/2\mathrm{i} \qquad S_{iz} = (n_{i\uparrow} - n_{i\downarrow})/2 \\ &S_i^\dagger = c_{i\uparrow}^\dagger c_{i\downarrow} \qquad\qquad S_i^- = c_{i\downarrow}^\dagger c_{i\uparrow} \end{aligned}$$

and $\theta_i = 2\phi_i$. When we apply this rotation to the Hamiltonian given by equation (5) and introduce the slave boson, we obtain

$$\begin{aligned} H = -t \cos\theta \sum_{i,j,\sigma} \hat{z}_{i\sigma}^\dagger \hat{z}_{j\sigma} f_{i\sigma}^\dagger f_{j\sigma} - t \sin\theta \sum_{i,j} \eta_i (\hat{z}_{i\uparrow}^\dagger f_{i\uparrow}^\dagger f_{j\downarrow} \hat{z}_{j\downarrow} - \hat{z}_{i\downarrow}^\dagger f_{i\downarrow}^\dagger f_{j\uparrow} \hat{z}_{j\uparrow}) \\ - \frac{1}{2}(h\cos\theta + \lambda^{(0)} \sin\theta) \sum_i (f_{i\uparrow}^\dagger f_{i\uparrow} - f_{i\downarrow}^\dagger f_{i\downarrow}) \\ - \frac{1}{2}(\lambda^{(0)} \cos\theta - h\sin\theta) \sum_i \eta_i (\hat{p}_{i\uparrow}^\dagger f_{i\uparrow}^\dagger f_{i\downarrow} \hat{p}_{i\downarrow} + \hat{p}_{i\downarrow}^\dagger f_{i\downarrow}^\dagger f_{i\uparrow} \hat{p}_{i\uparrow}) \end{aligned}$$

$$+ U \sum_i d_i^\dagger d_i - \frac{U}{2} \sum_{i,\sigma} f_{i\sigma}^\dagger f_{i\sigma} - \mu N - \frac{\lambda^{(0)} m_x}{2}$$
$$- \sum_i \lambda_i^{(1)} (e_i^\dagger e_i + p_{i\uparrow}^\dagger p_{i\uparrow} + p_{i\downarrow}^\dagger p_{i\downarrow} + d_i^\dagger d_i - 1)$$
$$- \sum_{i,\sigma} \lambda^{(2)} (f_{i\sigma}^\dagger f_{i\sigma} - p_{i\sigma}^\dagger p_{j\sigma} - d_i^\dagger d_i) \tag{8}$$

where we have omitted the primes. $\lambda^{(2)}$ and $\lambda^{(1)}$ are Lagrange multipliers enforcing the constraints of equation (3). In the above we have introduced the factors $\hat{z}_{i\sigma}$ and $\hat{p}_{i\sigma}$ given by

$$\hat{z}_{i\sigma} = \frac{1}{\sqrt{1 - p_{i\sigma}^\dagger p_{i\sigma} - d_i^\dagger d_i}} z_{i\sigma} \frac{1}{\sqrt{1 - e_i^\dagger e_i - p_{i\bar{\sigma}}^\dagger p_{i\bar{\sigma}}}} \tag{9}$$

$$\hat{p}_{i\sigma} = \frac{1}{\sqrt{1 - p_{i\sigma}^\dagger p_{i\sigma} - d_i^\dagger d_i}} p_{i\sigma} \frac{1}{\sqrt{1 - e_i^\dagger e_i - p_{i\bar{\sigma}}^\dagger p_{i\bar{\sigma}}}} \tag{10}$$

and $z_{i\sigma} = e_i^\dagger p_{i\sigma} + p_{i\bar{\sigma}}^\dagger d_i$. This choice of operators $\hat{z}_{i\sigma}$ and $\hat{p}_{i\sigma}$ guarantees the correct behaviour of the model in the $U \to 0$ limit [5].

In the following we make the saddle-point approximation for the Bose fields, replacing them by their mean (and site-independent) values, which results in the appearance of two elements: the band-narrowing factor q and a factor g changing the effective chemical potential and superconducting gap:

$$q = \langle \hat{z}_{i\sigma}^\dagger \hat{z}_{j\sigma} \rangle \tag{11}$$

$$g = \langle \hat{p}_{i\sigma}^\dagger \hat{p}_{i\bar{\sigma}} \rangle. \tag{12}$$

With the use of the electron–hole transformation and the requirement that the magnetization at each site points along the z-axis, we can express q and g as

$$q = \frac{4d^2}{1 - m^2} \left(1 - 2d^2 + \sqrt{(1 - 2d^2)^2 - m^2}\right) \tag{13}$$

$$g = \frac{2}{1 - m^2} \sqrt{(1 - 2d^2)^2 - m^2} \tag{14}$$

where $m^2 = m_z^2$ in the normal phase and $m^2 = m_z^2 + m_x^2$ in the ordered (superconducting) phase, respectively. The double occupancy (single occupancy in the attractive Hubbard model) is $d^2 = \langle d_i^\dagger d_i \rangle$ and

$$\tan\theta = m_x / m_z. \tag{15}$$

The resulting Hamiltonian is quadratic in fermion operators and can be diagonalized by the standard Bogolyubov-type transformation. Finally, the bosonic averages, the variational parameters and the rotation angle are calculated by extremizing the free energy.

In the normal phase, $\lambda^{(0)} = \theta = 0$ and the free energy per lattice site takes the following form [10]:

$$F_N = -\frac{2}{N\beta} \sum_k \ln \left\{ 2 \cosh \left[\frac{\beta}{2} (q\varepsilon_k - h/2) \right] \right\} + Ud^2 + (h - U) m_z/2 - U/2. \tag{16}$$

In the superconducting state,

$$F_S = -\frac{2}{N\beta} \sum_k \ln \left[2 \cosh \left(\frac{\beta E_k}{2} \right) \right] + Ud^2 - Un/2 + hm_z/2 + \lambda^{(0)} m_x/2 \tag{17}$$

$$E_k = \sqrt{(q_0\varepsilon_k - h_1)^2 + (q_1\varepsilon_k + \lambda_1)^2} \tag{18}$$

$$h_1 = \frac{hm_z + \lambda^{(0)}m_x}{2m} \qquad \lambda_1 = g\frac{\lambda^{(0)}m_z - hm_x}{2m} \qquad q_0 = q\frac{m_z}{m} \qquad q_1 = q\frac{m_x}{m} \tag{19}$$

with $m_x = m\sin\theta$, where θ is defined by equation (15), and $\beta = 1/k_BT$. The equations for m_x, h, $\lambda^{(0)}$ and d^2 are obtained by minimizing the free energy F_S and then they are solved self-consistently for a given band structure. We can obtain analogous equations, leading to the same results, in the negative-U Hubbard model, without resorting to the electron–hole transformation. The derivation is given in the appendix.

Let us note that an equivalent procedure at the SBMFA level consists in choosing the spin- and charge-rotationally invariant version of the slave-boson method of Frésard and Wölfle [12] (see also [11]). To establish this equivalence, we transform the quasiparticle energy E_k, with new fields η and δ, into the form

$$E_k = \sqrt{(q\varepsilon_k - \eta)^2 + \delta^2} \tag{20}$$

$$\eta = h_1\cos\theta - \lambda_1\sin\theta \tag{21}$$

$$\delta = h_1\sin\theta + \lambda_1\cos\theta. \tag{22}$$

The free-energy equation (17) can be expressed as

$$F_S = -\frac{2}{\beta N}\sum_k \ln\left[2\cosh\left(\frac{\beta}{2}E_k\right)\right] + Ud^2 - Un/2 + \eta m_z + \delta m_x. \tag{23}$$

This is the form obtained for the spin- and charge-rotationally invariant version of slave bosons [11]. If we treat η and δ as variational parameters, we get equations appropriate for this method, and the results obtained are exactly the same as in our approach. Thus, the two methods are strictly equivalent at the SBMFA level. In fact, at this level, global rotation of spin operators restores the rotational invariance.

The superconducting energy gap is 2δ if η is within the band, or is given by $2E_k$ evaluated for $\varepsilon_k =$ lower band boundary, if η falls below the bottom of the bare band.

For the sake of comparison, we also give the HFA solution for the Hubbard model equation (1) for the superconducting state:

$$F_S^{HF} = \bar{\mu}(n-1) - \frac{U}{4}n^2 + \frac{|\Delta|^2}{U} - \frac{2}{\beta N}\sum_k \ln[2\cosh(\beta E_k/2)] \tag{24}$$

$$n - 1 = -\frac{1}{N}\sum_k \frac{\bar{\varepsilon}_k}{E_k}\tanh(\beta E_k/2) \tag{25}$$

$$\frac{1}{U} = \frac{1}{N}\sum_k \frac{1}{2E_k}\tanh(\beta E_k/2) \tag{26}$$

where

$$E_k = \sqrt{\bar{\varepsilon}_k^2 + \Delta^2} \qquad \Delta = Ux_0 \qquad x_0 = |\langle c_{i\uparrow}^\dagger c_{i\downarrow}^\dagger\rangle|$$

$$\bar{\varepsilon}_k = \varepsilon_k - \bar{\mu} \qquad \bar{\mu} = \mu + \frac{U}{2}n. \tag{27}$$

We should point out that at $n = 1$ the superconducting state (SS) and charge-density-wave (CDW) state are strictly degenerate due to the SO(4) symmetry of the Hubbard model and can coexist with arbitrary weights [2, 4, 13]. While this special symmetry point can be incorporated in our approach, in the following we shall concentrate on the superconducting state only.

2.1. Electromagnetic properties

As far as the electromagnetic properties are concerned, we shall calculate two quantities: the London penetration depth λ, measuring the extent of the penetration of the magnetic field into the superconductor, and the Ginzburg–Landau coherence length ξ.

In the linear response theory the relation between the current $J_\alpha(\boldsymbol{k}, \omega)$ and the applied vector potential $A_\alpha(\boldsymbol{k}, \omega)$ ($\alpha = x, y, z$) is given by

$$J_\alpha(\boldsymbol{k}, \omega) = N\frac{c}{4\pi}\sum_\beta [\delta_{\alpha\beta} K_\alpha^{\text{dia}} + K_{\alpha\beta}^{\text{para}}(\boldsymbol{k}, \omega)]A_\beta(\boldsymbol{k}, \omega) \tag{28}$$

where K_α^{dia} and $K_{\alpha\beta}^{\text{para}}$ are the diamagnetic and paramagnetic parts of the response kernel. In the static limit ($\omega = 0$), λ is determined by the transverse part of the total kernel and in the ground state it can be given by the formula

$$\lambda = \frac{1}{\sqrt{-K^{\text{dia}}}} \tag{29}$$

where K^{dia} is the diamagnetic part of the response kernel. K^{dia} can be expressed as

$$K^{\text{dia}} = \frac{8\pi e^2}{\hbar^2 c^2 a^{d-2}}\frac{\langle E_{\text{kin}}\rangle}{zN} \tag{30}$$

where z is the coordination number, a is the lattice constant and E_{kin} is the hopping part of equation (1). In the slave-boson approach the mean kinetic energy is given by the formula

$$\langle E_{\text{kin}}\rangle = q\frac{\partial F_s}{\partial q}. \tag{31}$$

Let us note that, at $T = 0$ K, the formula $-K^{\text{dia}} = 1/\lambda^2$ gives the value of the superfluid density ρ_s; a non-zero value corresponds to the Meissner effect.

The Ginzburg–Landau coherence length (i.e. the spatial extent of the superconducting order parameter) can be obtained through the relation [14]

$$\xi = \frac{\Phi_0}{2\pi\sqrt{2}\lambda H_c} \tag{32}$$

where $\Phi_0 = hc/2e$ is the quantum flux, and the thermodynamic critical field H_c can be calculated from

$$\frac{H_c^2}{8\pi} = \frac{F_n - F_s}{Na^d}. \tag{33}$$

3. Results

For the numerical results presented below (at $T = 0$ K), we will use two sets of units: either t for all lattice structures or half of the bandwidth D, which is $2t$ for $d = 1$, $4t$ for $d = 2$, $6t$ for a sc lattice and $8t$ for a bcc lattice. If the unit is not stated explicitly, we are using the half-bandwidth unit. This unit is more suitable for comparisons of quantities among different lattices. It should be used especially in discussion of the crossover from the weak- to the strong-coupling limit. The bare t-unit permits us to compare the absolute values of a given quantity. Calculations using a rectangular density of states can be compared only with ones carried out using the D-unit.

The results for $d = \infty$ require a third set of units: $t^* = t\sqrt{2d} \equiv 1$. When expressed in this unit the calculated quantities for different lattices converge as the lattice dimensionality increases.

For infinite dimensionality we use the Gaussian density of states:

$$\rho(\epsilon)_\infty = \frac{1}{\sqrt{2\pi}t^*}\exp(-\epsilon^2/2t^*). \tag{34}$$

In one dimension,

$$\rho(\epsilon)_{1\mathrm{D}} = \frac{1}{2t\pi}\frac{1}{\sqrt{1-(\epsilon/2t)^2}} \tag{35}$$

for $|\epsilon/2t| < 1$ and is zero otherwise. For two dimensions the density of states is given by

$$\rho(\epsilon)_{2\mathrm{D}} = \frac{1}{2t\pi^2}\mathcal{K}(1-(\epsilon/4t)^2) \tag{36}$$

for $|\epsilon/4t| < 1$ and is zero otherwise, where $\mathcal{K}$ is the complete elliptic integral of the first kind. In three dimensions, for the sc, fcc and bcc lattice structures, we use the analytical approximation to the densities of states as calculated numerically by Jelitto [15]. Due to the electron–hole symmetry of the model, all of the concentration dependences are symmetric with respect to the change $n \to 2-n$, so they will be given for the range $\langle 0; 1\rangle$ of electron densities only.

Henceforth, by stating that $d = 3$ we will mean that we are considering a sc lattice, if not stated explicitly otherwise, and by saying $d = 2$ we will mean that we are considering a two-dimensional square lattice.

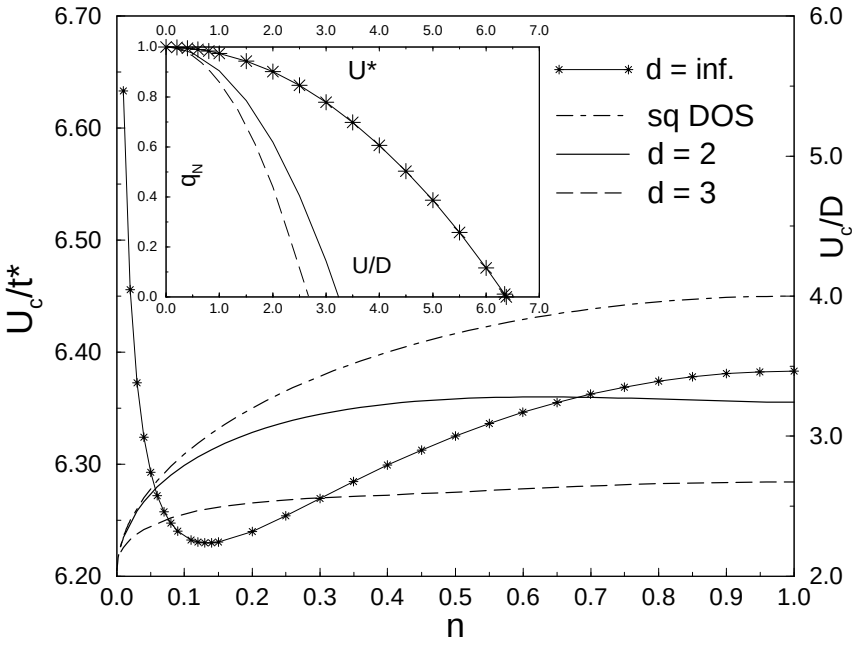

Figure 1. The critical value U_c/D versus the electron concentration n in the normal state for lattices of dimension $d = 2, 3, \infty$ and a square DOS. The inset shows the band-narrowing factor for the normal state versus U/D, and versus U^* for $d = \infty$, at half-filling. For infinite dimensions the appropriate scales are to the left of the main figure and at the top of the inset.

3.1. The normal state

In the normal phase, for a given electron density, both the single occupancy d^2 and the band-narrowing factor q decrease with increasing $|U|$. When q reaches 0 at half-filling for a certain (positive) U_c, we obtain a metal–insulator transition. In the case of attractive on-site interaction, U_c depends on the electron density in the way shown in figure 1. The values of U_c/D at $n = 1$ are 3.24228 and 2.67313, respectively, for $d = 2$ and $d = 3$ sc lattices, 2.61688 for fcc lattices and 2.06458 for bcc lattices. For a rectangular band of width $2D$, U_c increases monotonically from 0 to 4 at half-filling according to the formula

$$U_c/2D = 1 + \sqrt{n(2-n)}.$$

The characteristics for the real densities of states are flatter. U_c/D rises sharply for low electron densities and changes little for intermediate densities to reach the values given above at half-filling. The range of interaction (D-units) for which hopping is not yet suppressed is larger for a $d = 2$ square lattice than for a $d = 3$ sc lattice (see the inset in figure 1). In t-units the order is reversed: U_c/t is smaller for $d = 2$ and larger for $d = 3$. The case of infinite dimensions cannot be directly compared to the previous ones due to the different choice of units, which will be discussed further. With decreasing electron density, U_c gets smaller for finite-dimensional lattices, but for $d = \infty$, U_c sharply rises; this is connected with the infinite bandwidth in this case. This shows possible restrictions of the infinite-dimensions approximation for low electron densities (which is also seen in figure

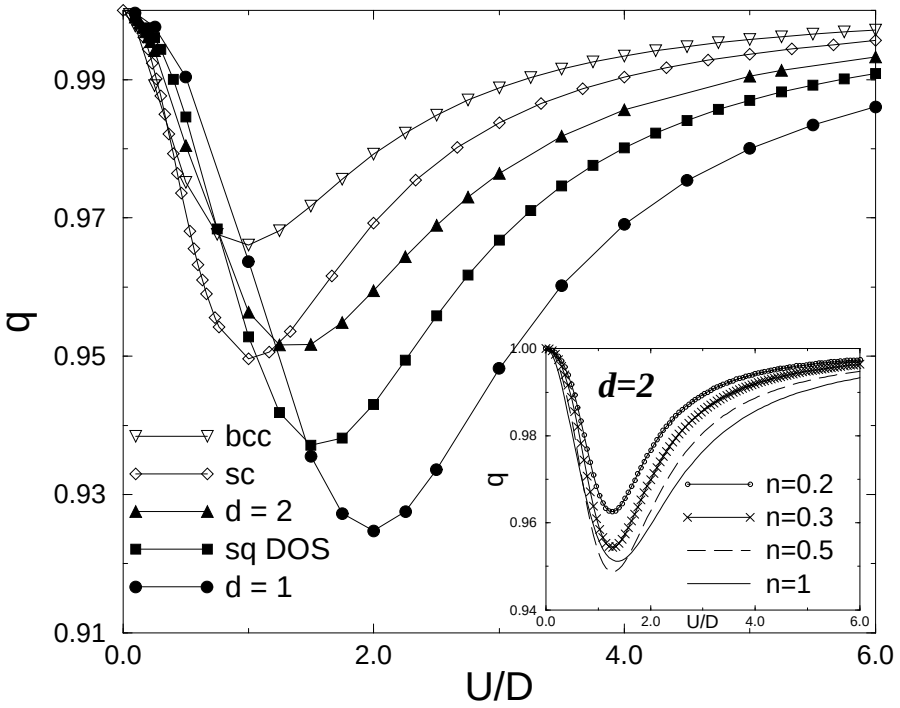

Figure 2. The band-narrowing factor q for the superconducting state versus the on-site interaction U/D at half-filling for a $d = 1$ lattice, a $d = 2$ square lattice, bcc and sc lattices and a square DOS. In the inset, the factor q for a two-dimensional square lattice is plotted for the particle densities $n = 0.2$, $n = 0.3$, $n = 0.5$ and $n = 1$.

20 in section 3.5).

Let us note, however, that for lattice dimensionalities larger than one, the ground state is superconducting (or with coexisting SS and CDW ordering for $n = 1$) and its properties will be discussed next.

3.2. The superconducting state

The band-narrowing factor q versus U/D is plotted in figure 2 for $n = 1$. The value $q = 1$ is the HFA result. The deviation of q from 1 reflects the effect of local correlations, which are taken into account in the SBMFA approach. As we see, there is a certain value of U for which this deviation is the strongest. This U-value grows with decreasing lattice dimensionality. We note the weaker influence of local correlations in the case of the square lattice with the exact DOS than in the case of the square lattice with the rectangular DOS. Although for any n, q is close to 1, in contrast to the behaviour of q in the normal state, these small differences are responsible for the stability of the superconductivity for weak and intermediate coupling and for the differences between the slave-boson results and the HFA.

There is an interesting feature concerning the $d = 2$ square lattice (see the inset in figure 2) and the bcc lattice: both lattices exhibit van Hove singularity at half-filling. While for other lattices, q grows with decreasing n, for these two, q decreases when we move away from half-filling. The minimum is reached at around $n \sim 0.5$ and when we decrease n further, q increases. This feature may be connected with the decrease of the superfluid density for the two-dimensional square lattice in the range $n \in \langle 0.8, 1\rangle$ (see figure 14, later). Let us note that this irregularity is not visible in the behaviour of other calculated quantities, due to the dominant influence of the mean-field approximation.

The results for the energy gap in one dimension ($d = 1$) are given in figure 3, where we plot the gap versus the electron concentration. We show plots for different values of the

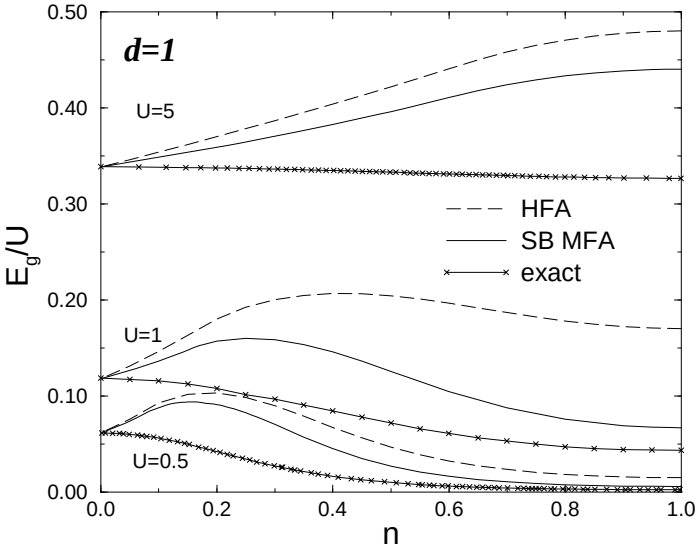

Figure 3. Exact, HFA and SBMFA values of the ratio of the energy gap to the on-site interaction U versus the electron concentration n for $d = 1$ for $U/D = 0.5$, $U/D = 1$, $U/D = 5$. The exact results are from Marsiglio [16].

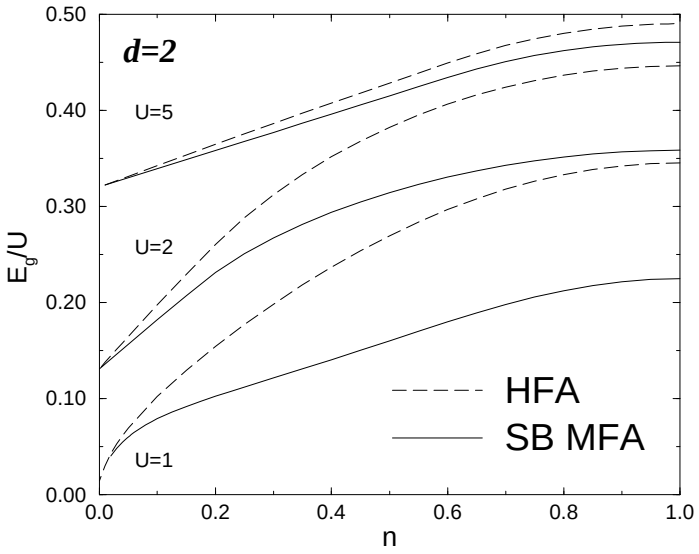

Figure 4. HFA and SBMFA values of the ratio of the energy gap to the on-site interaction U versus the electron concentration n for the $d = 2$ square lattice for $U/D = 1$, $U/D = 2$, $U/D = 5$.

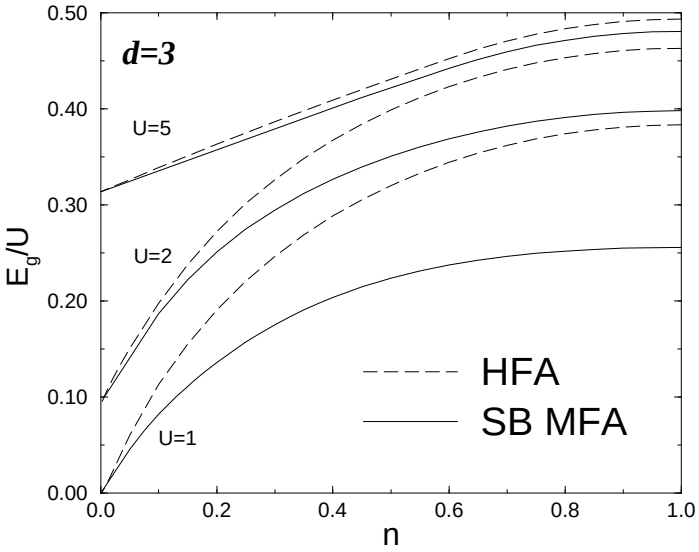

Figure 5. HFA and SBMFA values of the ratio of the energy gap to the on-site interaction U versus the electron concentration n for the $d = 3$ sc lattice for $U/D = 1$, $U/D = 2$, $U/D = 5$.

on-site interaction U/D, calculated in both the HFA and the SBMFA. They are compared with the exact results based on the Bethe *ansatz* calculations made by Marsiglio [16]. The HFA results for the energy gap are rather poor, giving non-monotonic dependence on the electron density n, in sharp contrast to the monotonic behaviour of the exact solution. Also, the HFA numerical values are up to five times higher, the difference being the largest at half-filling. It is of interest that for $d = 1$, the Bardeen–Cooper–Schrieffer HFA is a very

good approximation to the ground-state energy but it yields incorrect results in the evaluation of the energy gap [16, 17], except for in the case of the zero-density limit. The SBMFA solution is closer to the exact one, although, in general, with a shape resembling that of the HFA non-monotonic solution. The numerical value of the gap in the weak-coupling limit for $n = 1$ in the SBMFA can be up to 150% of the exact one (compared to about 400% in the HFA) in the weak-coupling limit. For strong coupling the SBMFA gap becomes closer to the HFA results but the quantitative correction is still quite large. This difference between the SBMFA and the exact results most probably stems from the nature of the ground state for $d = 1$ which does not exhibit long-range order.

The results concerning the superconducting phase for $d = 2$ and $d = 3$ lattice structures are shown in figures 4 and 5 and they exhibit similar behaviour. For $n \to 0$ they go over to the exact ones, i.e. the energy gap for $d = 2$ is just half of the binding energy for two electrons in an empty lattice. However, for $d = 3$, $E_g \to 0$ for $U/D = 1$, because a real bound state for the sc lattice is formed only for $U/D > 1.318$ [2].

Figure 6 shows the ratio of the SB energy gap to the HF energy gap for a half-filled band. With increasing on-site interaction this ratio tends to 1 and for large U the largest corrections are for $d = 1$; they are smaller for $d = 2$ and smallest for $d = 3$. This sequence is valid also for intermediate values of U, but when U/D approaches 0, the curve for $d = 2$ steeply increases and becomes larger than the ratio for $d = 3$, due to the van Hove singularity for $d = 2$. In t-units the corrections increase with dimensionality in the strong-coupling limit. With decreasing U/t the corrections in one dimension become dominant, irrespective of the set of units used. The largest differences between the energy gap calculated in the SBMFA and in the HFA are for small and intermediate values of the on-site interaction U. In the inset the same quantity is shown versus the electron density

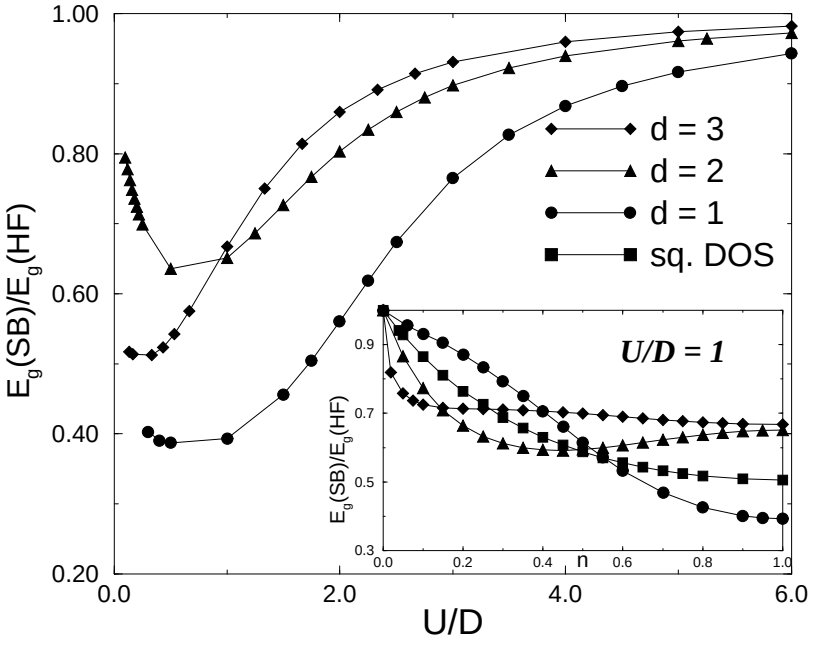

Figure 6. The ratio of the SBMFA energy gap to the HFA energy gap versus the on-site interaction U/D at half-filling for $d = 1$ and $d = 2$ square lattice and sc lattice structures. In the inset the same ratio versus n for fixed $U/D = 1$ with a square-DOS curve added is shown.

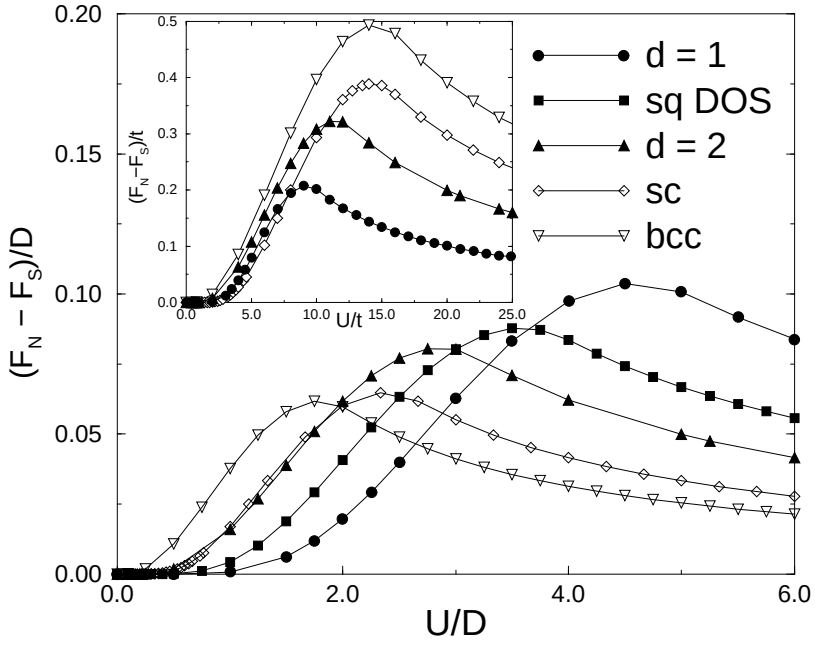

Figure 7. The condensation energy in half-bandwidth units versus the on-site interaction U/D at half-filling for $d = 1$ and $d = 2$ square lattices, a square DOS, and $d = 3$ sc and bcc lattices. It is shown in t-units in the inset.

n, for fixed $U/D = 1$. For small densities the sequence of curves reverses: one dimension yields the smallest corrections and a sc lattice the largest—exactly opposite to the situation for an approximately half-filled band.

The free-energy difference between the normal and the superconducting states (ΔF) (i.e. the condensation energy) at half-filling is displayed for various lattices in figure 7. Like in the q versus U plot, the highest extremum is for $d = 1$ (in D-units). The maximum of the free-energy difference shifts towards lower values of U/D with increasing lattice dimensionality, but it does not coincide with the points where the band-narrowing factor is a minimum. In three dimensions the peaks of the condensation energy are approximately of the same value for the bcc and sc lattices, but the value of U/D for which the first one appears is smaller than that at which the latter appears.

Using t-units, we see that changing the coordination number without changing the dimensionality (bcc to sc) makes the minima differ in value but they appear for the same U/t coordinate. The larger the coordination number of a given lattice, the larger the value of the maximum and the value of U/t at which it appears. For the other electron densities the condensation energy versus U behaviour is qualitatively similar (see figures 8 and 9). The maximum of ΔF, although it lowers with decreasing n, remains almost unchanged relative to the U-coordinate and only for very low electron densities does it start to move towards weak-coupling U-values, thus extending the strong-coupling regime. Finally, we note that figure 7 also shows a change of the thermodynamic critical magnetic field with U according to the relation given by equation (33). Our results for the free-energy difference and H_c^2 in the SBMFA are much more realistic than those in the HFA, since the latter neglects the effects of local correlations in the normal state and grossly overestimates the condensation energy (see also references [10, 11]). Let us recall that the SBMFA agrees

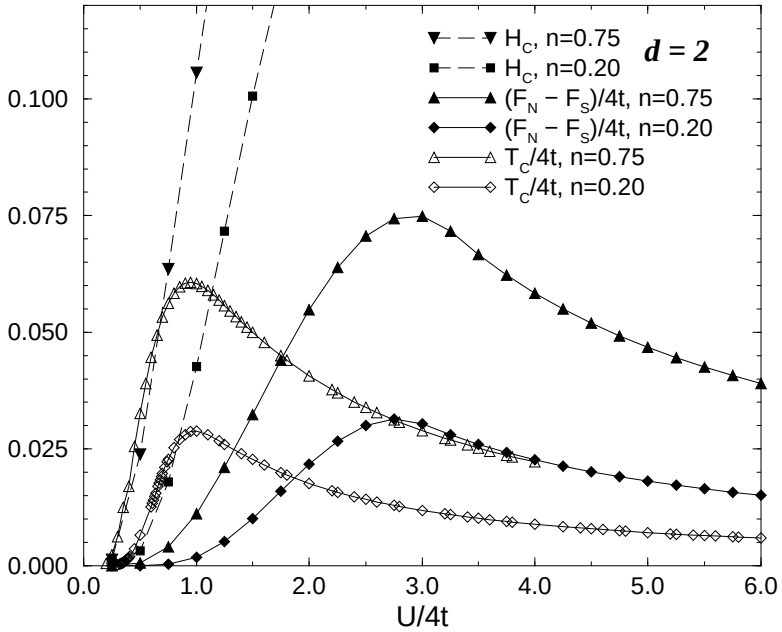

Figure 8. The Kosterlitz–Thouless critical temperature (T_c), the condensation energy ($F_N - F_S$) and the critical magnetic field (H_c) versus the on-site interaction $U/4t$ for a $d = 2$ square lattice for the electron densities $n = 0.2$ and $n = 0.75$.

with a perturbational treatment both in the weak- and strong-coupling limits [5, 9] while this is the case for the HFA only for the weak-coupling limit.

In the slave-boson approach to the Hubbard model, the calculation of the superconducting critical temperature is not straightforward. We can ask, however, whether the dependences of a condensation energy in the ground state versus the coupling strength and density can be approximations of analogous variations of the critical temperature. The answer is depicted in figures 8, 9, 10. We have plotted the results of the alloy-analogy approximation to the functional-integral method for $d = 3$ given by Hasegawa [19] together with the results obtained by using the linked-cluster expansion, the high-temperature series expansion of the Heisenberg model with $s = 1/2$ and the molecular-field approximation of [20] (figure 9), Monte Carlo calculations for $d = \infty$ given by Jarrell [21] (figure 10) and numerical results for T_c from the Kosterlitz–Thouless (KT) transition for $d = 2$ (figure 8), together with plots of the free-energy difference in the ground state. We remind the reader that, by the canonical transformation method, the attractive Hubbard model in the strong-coupling limit ($|U| \gg t$) can be mapped onto the effective pseudospin Heisenberg model with $s = 1/2$, with the single occupancies excluded [2, 13].

As far as the $d = 2$ case is concerned, we note that the model undergoes the KT transition away from half-filling. In order to determine T_c in 2D we have used the relation for the universal jump of the superfluid density ρ_s (evaluated below T_c) [18]:

$$\rho_s^-(T_c) = \frac{2}{\pi} k_B T_c \tag{37}$$

where

$$\rho_s(T) = -\frac{t}{N}\sum_k \left[\frac{\bar{\varepsilon}_k \cos(k_x)}{2E_k} \tanh(E_k/2k_BT) + \frac{t \sin^2(k_x)}{2k_BT \cosh^2(E_k/2k_BT)} \right] \tag{38}$$

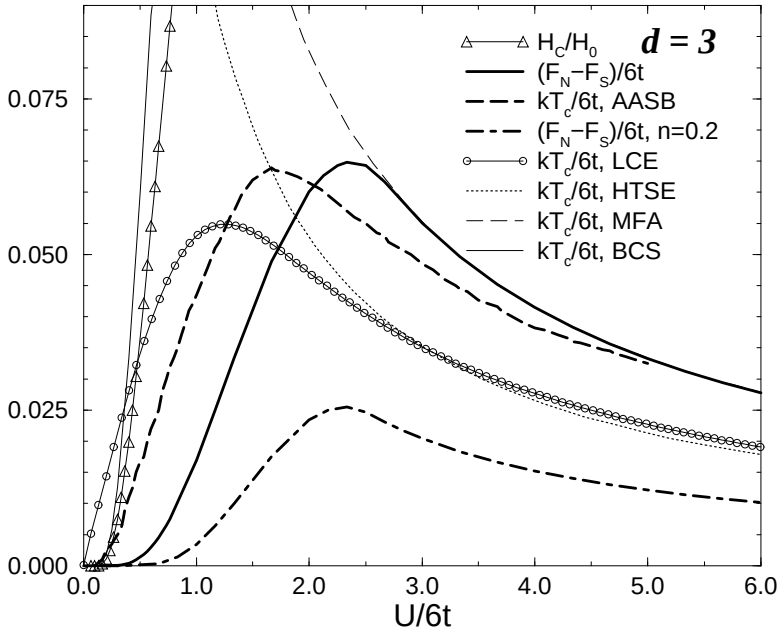

Figure 9. The critical temperature, the condensation energy and the critical magnetic field versus the on-site interaction $U/6t$ for a $d = 3$ sc lattice at half-filling together with the condensation energy for $n = 0.2$. AASB indicates the results obtained by using the alloy-analogy slave-boson approximation given by Hasegawa [19]; LCE, HTSE, MFA indicate the results obtained from the linked-cluster expansion, the high-temperature series expansion and the mean-field approximation, in the large-U limit, respectively, and these results were taken from the work of Pan and Wang [20]. Triangles show the thermodynamic critical field, the thick solid line shows the condensation energy and the fine solid line (BCS) shows the Bardeen–Cooper–Schrieffer (BCS) critical temperature.

with the notation of equation (27); Δ and $\overline{\mu}$ are calculated from the BCS equations (25) and (26).

The general shape of the curves and the absolute value of the maxima for $\Delta F(U)$ and $T_c(U)$ are comparable, but the maxima appear for different U-values. The critical temperature reaches the highest peak for lower values of U and is itself slightly smaller than, comparable to and slightly larger than the maxima of the free-energy difference for $d = 2$, $d = 3$ and $d = \infty$ respectively. In three dimensions, for the sc lattice the linked-cluster expansion yields a maximum of the critical temperature that is smaller and for smaller U-values than slave-boson mean-field results. In the large-U limit, the former agrees with the high-temperature series expansion of the Heisenberg model with $s = 1/2$ while the latter tends to the molecular-field approximation. The linked-cluster expansion, which is more reliable, indicates that the condensation energy in three dimensions is not as good an approximation of the critical temperature as we might infer from the mean-field calculations. Nevertheless, in the weak-coupling limit, the linked-cluster expansion becomes dubious, yielding results exceeding the BCS ones. In this limit the mean-field calculations are much better. From figures 8 and 9 we see that a decrease in the electron density considerably diminishes the values of the maxima of both quantities and the difference between them, but changes their positions on the U-axis only very weakly, the shift being noticeable only for very small densities. For smaller densities the maxima of both the condensation energy

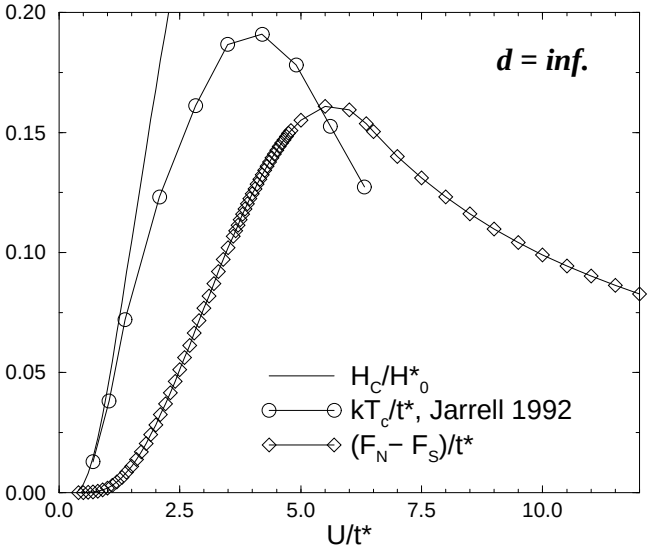

Figure 10. The critical temperature (from Jarrell [21]), the condensation energy and the critical magnetic field versus the on-site interaction U/t^* for $d = \infty$ at half-filling.

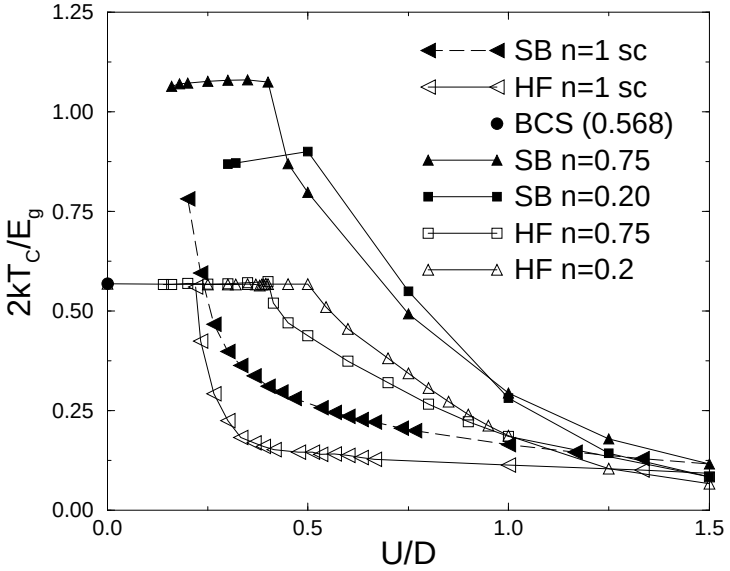

Figure 11. The ratio $2k_BT_c/E_g$ versus U/D for a $d = 3$ sc lattice at half-filling and for a $d = 2$ square lattice for band fillings of $n = 0.2, 0.75$ in the SBMFA and the HFA.

and the critical temperature appear for smaller U-values. Let us note that the slave-boson method yields the atomic-limit result for the normal state for sufficiently large U ($U > U_c$; see figure 1) while, as we know (e.g. [2]), there exist processes of the order of t^2/U in the strong-coupling limit. The resultant free-energy difference curves perpetuate this error in this range.

Additionally, figures 8–10 show the thermodynamic critical magnetic field H_c, in units

of

$$H_0 = \sqrt{8\pi D/a^d}.$$

H_c seems to be a reliable approximation to the critical temperature in the weak-coupling regime, especially for $d = 2$ and for smaller electron densities.

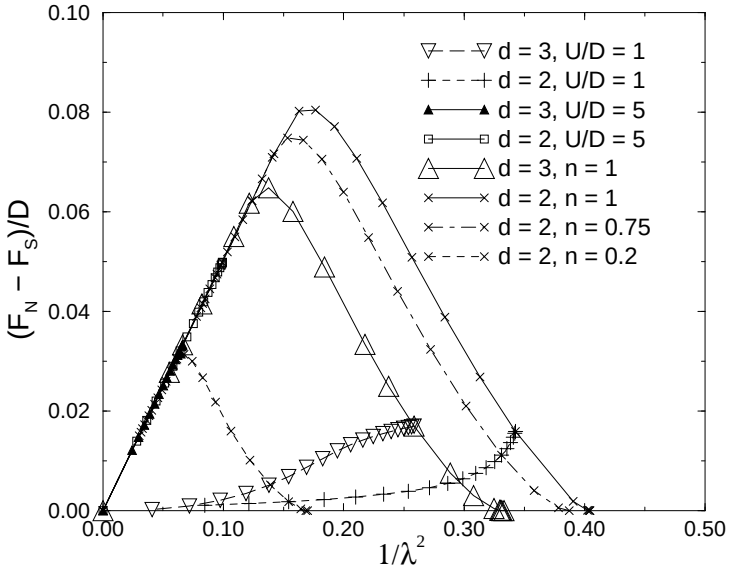

Figure 12. The condensation energy in half-bandwidth units versus $1/\lambda^2$ for a sc lattice and for a $d = 2$ square lattice, plotted for fixed n with U as a driving parameter of crossover as well as for fixed U with n as a driving parameter. For a sc lattice curves are for $U/D = 1$ and $U/D = 5$ with $n \in \langle 0, 1\rangle$ and at half-filling with $U/D \in \langle 0, 6\rangle$. For a $d = 2$ square lattice curves are for $U/D = 1$ and $U/D = 5$ with $n \in \langle 0, 1\rangle$ and for $n = 0.2$, $n = 0.75$ and $n = 1$ with $U/D \in \langle 0, 6\rangle$. λ is given in units of $\lambda_0 = \hbar c\sqrt{a^{d-2}z/8\pi D}/e$.

Knowing the values of the energy gap, it is of interest to determine the ratios $k_B T_c/E_g$ and compare them with the BCS value. In figure 11 there are plots of the ratio of the critical temperature to the energy gap versus U/D (T_c for a $d = 3$ lattice from [19] and for $d = 2$ from the KT transition). For large U the ratio quite quickly decreases, because T_c diminishes as shown in figures 8 and 9, while $\Delta \approx U$ in this limit. With decreasing U, the ratio grows until it reaches the point at which a decrease in U does not change the value of the ratio, which in the HFA takes the BCS value 0.568, irrespective of the lattice dimensionality (see Czart *et al* [22]). In the SBMFA the ratio decreases slightly when we approach $U = 0$, reaching a value of $0.568E_g(\mathrm{HF})/E_g(\mathrm{SB})$, larger than the BCS one. Notice, however, that we have used the same value of T_c, evaluated in the KT scenario (through the BCS approximation for the superfluid density), but that the energy gap values are from HFA and SBMFA treatments, respectively. The U-value for which the ratio becomes constant in the HFA, or approximately constant in the SBMFA, decreases with growing electron density. This U-value, in D-units, is also smaller for a $d = 3$ lattice than for a $d = 2$ one.

3.3. Scaling properties

Although, as we have discussed before, the condensation energy in general does not quantitatively determine the behaviour of the critical temperature, we have plotted ΔF

versus the superfluid density $1/\lambda^2$ to obtain a Uemura-type plot [7] and searched for scaling properties. The outcome is shown in figure 12. Results of many different calculations for different U and n fit perfectly on our Uemura-type plot. The free-energy difference is proportional to the superfluid density up to a certain value where it reaches a peak and then decreases. The absolute value of the peak and its superfluid density coordinate depend on U, n and the dimensionality of the lattice. For a three-dimensional lattice the maximum of the free-energy difference is lower than for a two-dimensional one at the same electron concentration (assuming the same value of the hopping integral t for the two cases). The plots were extracted from the results for ΔF and λ versus U and n. In the curves calculated for a constant electron density, a decrease in the superfluid density is equivalent to an increase in the absolute value of the on-site interaction U. The peak is reached for $U/D \sim 2.3$ for a sc lattice with a half-filled band and about 2.8 for $d = 2$—these values are approximately the same at all densities n examined. This is in agreement with our results for the critical temperature for $d = 2$, which show that the peak of T_c is reached at about the same value of U over a very broad range of electron densities. When we further increase U we move to the part of the curve of constant slope and ΔF decreases to 0 for large U. This is the part of the plot corresponding to low superfluid densities where the slopes of all of the curves take a universal value.

Our plot resembles that of Uemura only for large U, as expected, because the characteristic dependence of T_c on $1/\lambda^2$ was found only for type II superconductors, with strong pairing and short coherence lengths. For small U we do not obtain the universal slope with decreasing n, and the plots are non-universal. For U large enough, the behaviour is universal for all possible electron densities.

For the sake of comparison, a plot of the critical temperature versus $1/\lambda^2$ for $d = 2$ for $n = 0.75$ is shown in figure 13. For both curves, T_c comes from the Kosterlitz–Thouless

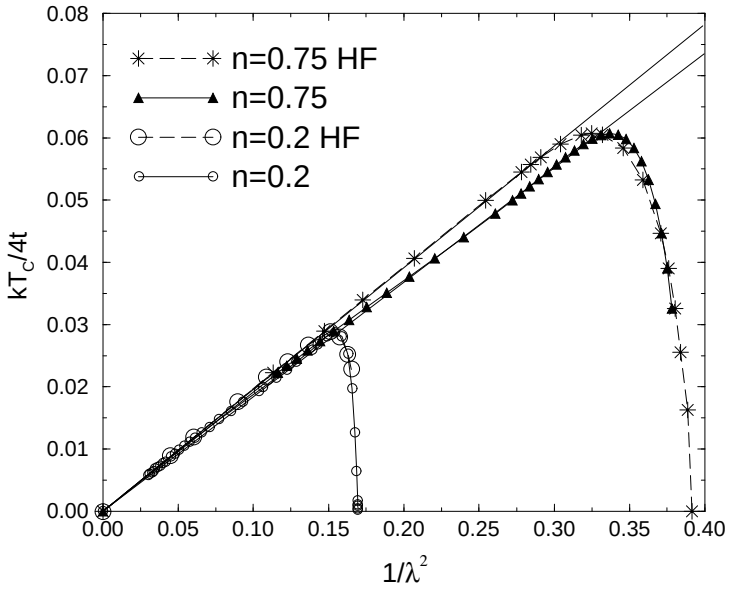

Figure 13. The Kosterlitz–Thouless critical temperature versus $1/\lambda^2$ for a $d = 2$ square lattice, for band fillings of $n = 0.2$ and $n = 0.75$ in the HFA and the SBMFA. Straight lines show the universal slope in the two approximations. λ is given in units of $\lambda_0 = \hbar c\sqrt{a^{d-2}z}/8\pi D/e$.

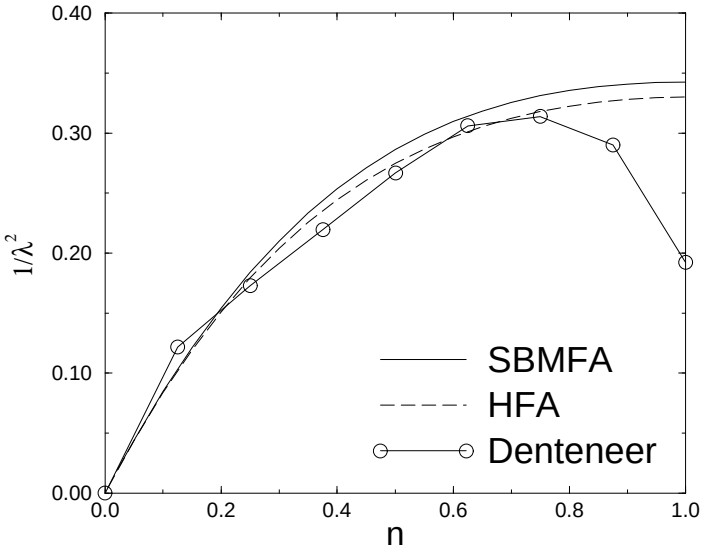

Figure 14. The superfluid density $1/\lambda^2$ versus the electron concentration for a $d = 2$ square lattice for $U/4t = 1$ in the HFA and SBMFA, together with the results obtained using the exact-diagonalization method by Denteneer [23]. λ is given in units of $\lambda_0 = \hbar c\sqrt{a^{d-2}z/8\pi D}/e$.

transition and λ from the HF or SB approximations. For a fixed U an increase in the superfluid density is equivalent to an increase in electron density. Both methods yield the universal behaviour in the strong-coupling limit. BCS-HFA points create a line slanting at the angle $\pi/2$ (with the factor $1/8$ included in the definition of λ), while SBMFA points create one slanting at a slightly smaller angle. This angle is smaller than in the case of condensation energy versus $1/\lambda^2$ and the decreasing branch descends much more steeply. Comparing the HFA and SBMFA, we see that the BCS-HFA method produces a slightly higher transition temperature for a given λ in the 'underdoped' region (to the left of the maximum) and a slightly smaller one in the 'overdoped' region (to the right of the maximum) than the SBMFA method. This difference is not large, like the difference between the λ-values evaluated in the HFA and SBMFA.

3.4. Electromagnetic properties

The electromagnetic properties are shown in figures 14–18 (H_c in figures 8–10). The London penetration depth λ determined in the SBMFA does not differ much from the results for the HFA (we calculate λ in units of $\lambda_0 = \hbar c\sqrt{za^{d-2}}/e\sqrt{8\pi D}$). A plot of the inverse square of λ (the superfluid density) is given in figure 14, together with the results obtained using the exact-diagonalization method by Denteneer [23] for a 4×4 lattice. The simple HF approach is good over a wide range of electron densities from 0 to about 0.8, with the SBMFA results being only slightly larger. The discrepancies between the two curves and the exact-diagonalization results appear at around $n = 0.8$. At this density, ρ_s from the exact-diagonalization method begins to decrease, while ρ_s in the HFA or SBMFA monotonically increases with the electron density, reaching a maximum at half-filling. The two different kinds of behaviour appear because in both the HFA and the SBMFA the effect of the current–current correlations is neglected, and short-range CDW correlations, important close to half-filling, are not taken into account.

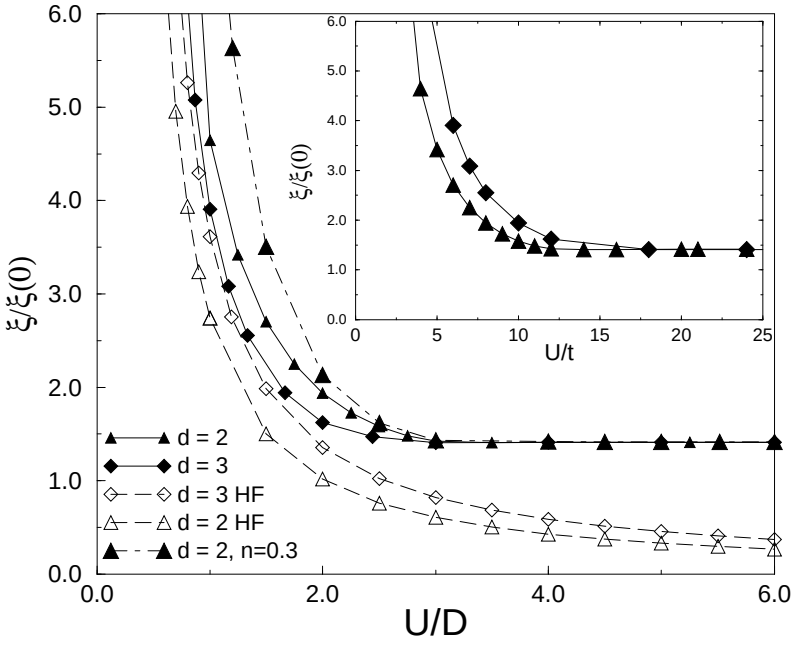

Figure 15. The Ginzburg–Landau coherence length $\xi/\xi(0)$ versus the on-site interaction U/D at half-filling for a $d = 2$ square lattice and a $d = 3$ sc lattice in the SBMFA and HFA. The inset shows the SBMFA plots of $\xi/\xi(0)$ for a $d = 2$ square lattice and a $d = 3$ sc lattice in t-units. $\xi(0) = a/2\sqrt{2z}$.

Let us now discuss the evolution of the correlation length. The Ginzburg–Landau (GL) coherence length ξ (in units of $\xi_0 = a/2\sqrt{2z}$), shown in figure 15, tends to a constant value $\sqrt{2}$ in the strong-coupling limit and diverges to infinity when U approaches 0. For a fixed U in the region of divergence, the $d = 2$ lattice yields larger values of ξ than the $d = 3$ lattice if we use D-units and smaller values if we use t-units.

The ξ-dependence on the electron density for $U/D = 1$ (figure 16) is qualitatively different for different lattices: ξ decreases when n approaches the half-filled band for sc and $d = 2$ lattices and increases for a square density of states. The HFA curve is very close to the slave-boson approach results for $d = 3$, but is lower by about 30% for $d = 2$ and is lower by up to 50% in the square-DOS case. ξ plotted for $d = \infty$ is a very good approximation to the $d = 3$ case for the range of electron densities 0.1–1. Changing to t-units (see the inset in figure 16) increases only the difference between the absolute values of ξ reached for $d = 2$ and $d = 3$ lattices.

Next, we compare the pair radius ξ_{pair} with the Ginzburg–Landau coherence length. ξ_{pair} can be evaluated as follows [24]:

$$\xi_{\text{pair}}^2 = \left(N^{-1}\sum_{\boldsymbol{k}} |\nabla\phi(\boldsymbol{k})|^2\right) \Big/ \left(N^{-1}\sum_{\boldsymbol{k}} |\phi(\boldsymbol{k})|^2\right) \tag{39}$$

where $\phi(\boldsymbol{k})$ is the 'internal pair wave function' determined in the BCS-HFA, i.e. $\phi(\boldsymbol{k}) = \Delta/2E_k$. It measures a pair radius in the BCS condensate (or more precisely, two-electron correlation) and in the $n \to 0$ limit it gives the bound-state radius for the two-electron

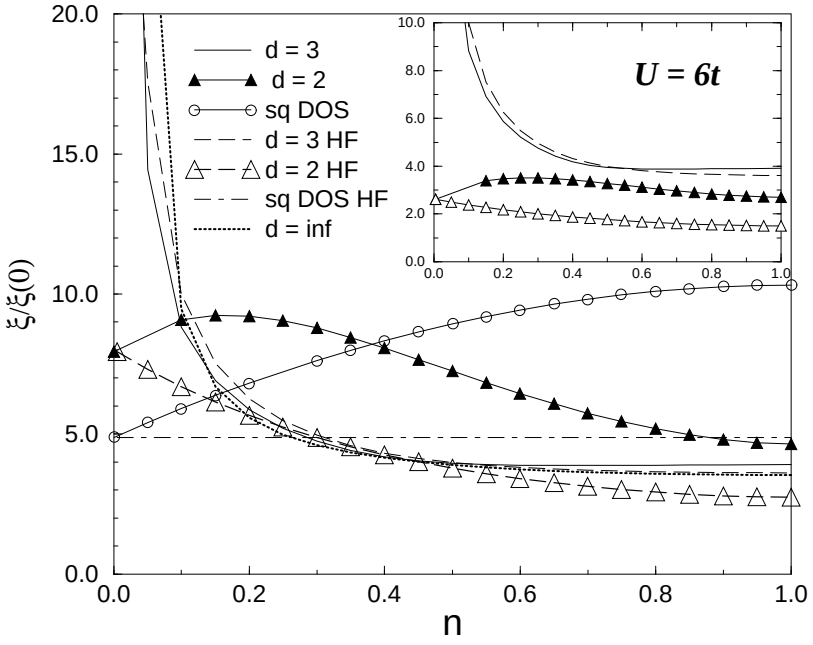

Figure 16. The Ginzburg–Landau coherence length $\xi/\xi(0)$ versus the electron concentration n in the SBMFA and HFA for $U/D = 1$ for a $d = 2$ square lattice, a $d = 3$ sc lattice, a square DOS and $d = \infty$ (only in the SBMFA). The inset shows the same plots in t-units for a $d = 2$ square lattice and a $d = 3$ sc lattice. $\xi(0) = a/2\sqrt{2z}$.

problem. For $d = 2$, ξ_{pair} can be expressed in terms of the complete elliptic integrals:

$$(\xi_{\text{pair}}/a)^2 = L_1/L_2 \qquad L_1 = \int \rho_1(\epsilon)/E(\epsilon)^6 \,\mathrm{d}\epsilon \qquad L_2 = \int \rho(\epsilon)/E(\epsilon)^2 \,\mathrm{d}\epsilon \tag{40}$$

$$\rho_1(\epsilon) = N^{-1}\sum_k (\nabla\varepsilon_k)^2\delta(\epsilon-\varepsilon_k) = \frac{8t}{\pi^2}\left[\mathcal{E}\left(1-\frac{\epsilon^2}{16t^2}\right) - \frac{\epsilon^2}{16t^2}\mathcal{K}\left(1-\frac{\epsilon^2}{16t^2}\right)\right] \tag{41}$$

for $|\epsilon/4t| < 1$, where $\mathcal{K}$ and $\mathcal{E}$ are the complete elliptic integrals of the first and second kind [25], respectively, and $E(\epsilon)$ and $\rho(\epsilon)$ are given by equation (27) and equation (36).

The plots of ξ_{pair} and the GL ξ are shown in figures 17 and 18. Although ξ_{pair} and the Ginzburg–Landau coherence length ξ are different lengths, it turns out that at half-filling they are very close to each other in the HFA (figure 17). A similar behaviour is observed over a wide range of electron densities for fixed U, from half-filling to about 0.1 (figure 18). For a large U the pair radius tends to zero together with the Ginzburg–Landau coherence length calculated within the HFA while the slave-boson calculations of the Ginzburg–Landau coherence length yield a finite and constant result. This is the correct result because the coherence length is finite even for a very small separation between the paired electrons.

3.5. The case where $d = \infty$

An interesting part of the present study concerns the infinite-dimensional case $d = \infty$. The idea was introduced by Metzner and Vollhardt [6] as an approximation of the $d = 3$ case, greatly simplifying the many-body calculations. For $d = \infty$ the SBMFA, which is equivalent to the Gutzwiller approximation of the Gutzwiller wave function, yields the

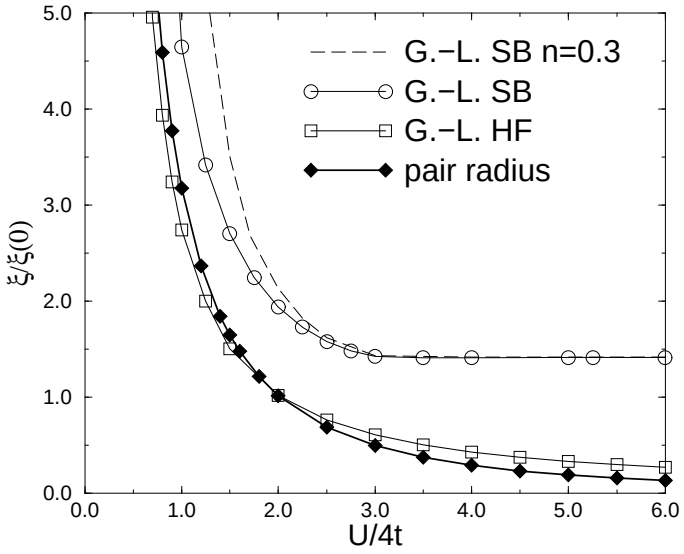

Figure 17. The Ginzburg–Landau coherence length $\xi/\xi(0)$ in the SBMFA and HFA and the pair radius versus the on-site interaction $U/4t$ for a $d = 2$ square lattice at half-filling and for the electron density $n = 0.3$. $\xi(0) = a/2\sqrt{2z}$.

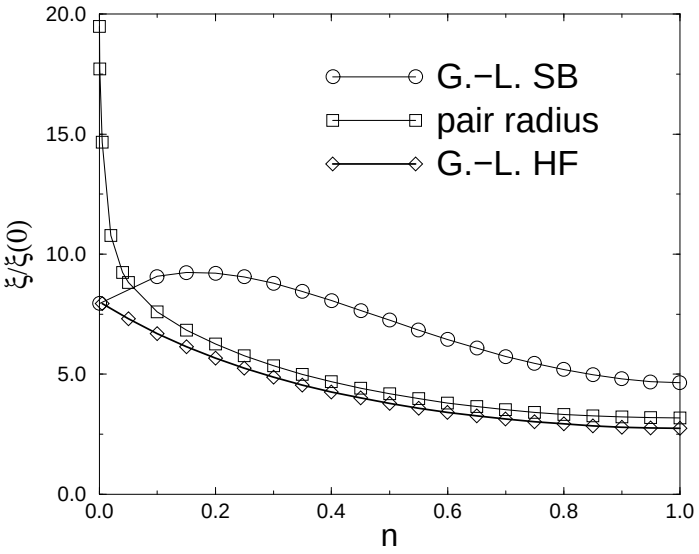

Figure 18. The Ginzburg–Landau coherence length $\xi/\xi(0)$ and the pair radius versus the electron concentration n for $U/4t = 1$ for a $d = 2$ square lattice in the SBMFA and HFA. $\xi(0) = a/2\sqrt{2z}$.

same results as the calculations with the use of the Gutzwiller wave function without the Gutzwiller approximation. To obtain finite results we have used renormalized units: $t^* = t\sqrt{2d} \equiv 1$, in accordance with the remark at the beginning of section 3. Figure 19 presents plots of the energy gap for different lattice dimensionalities for $U^* = U/t^* = \sqrt{6}$ (which for $d = \infty$ is smaller than U_c^* shown in figure 1). The plots converge to the plot

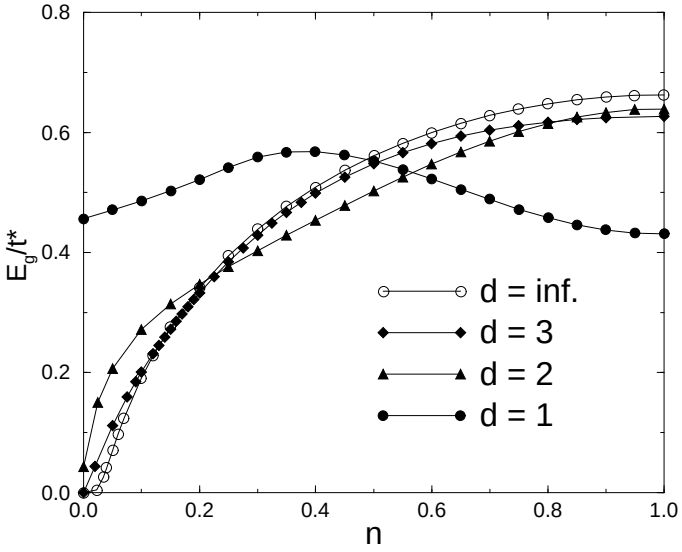

Figure 19. The energy gap in t^*-units versus the electron concentration n for $d = 1$ and $d = 2$ square lattices, a $d = 3$ sc lattice and a $d = \infty$ lattice, for $U/t^* = \sqrt{6}$ in the SBMFA.

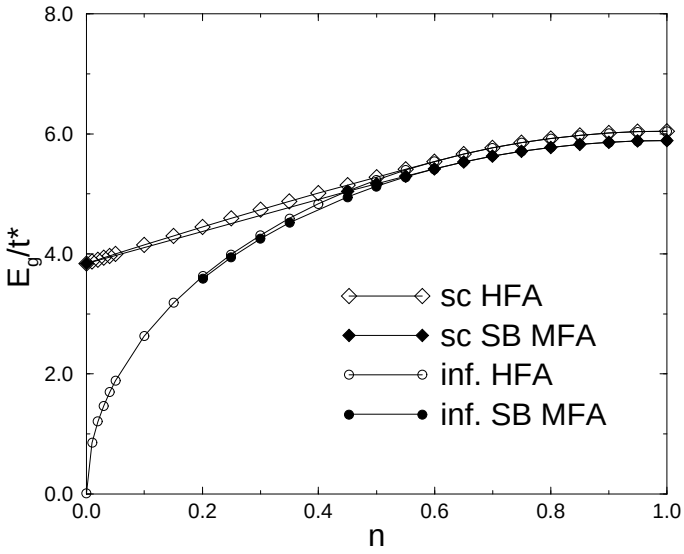

Figure 20. The energy gap in t^*-units versus the electron concentration n for a $d = 3$ sc lattice and $d = \infty$ for $U/t^* = 5\sqrt{6}$ in the SBMFA and the HFA.

for $d = \infty$ with increasing dimensionality and the results for $d = 3$ lie close to those for $d = \infty$. An exception is given in figure 20, where the curves are plotted for $U^* = 5\sqrt{6}$ (larger than U_c^* for $d = \infty$). In the infinite-dimensional case the bandwidth is infinite and a bound state cannot be formed, unlike in the $d = 3$ case. The plots converge only for intermediate densities and half-filling.

In general, we can say that the results for $d = \infty$ provide a good quantitative approximation to those from the calculations performed for $d = 3$. As far as the energy

gap behaviour is concerned, we notice that, unlike for the $d = 3$ case, electrons will never form a bound pair in an empty lattice for $d = \infty$ (figure 20).

4. Summary

We have carried out a ground-state analysis of the attractive Hubbard model for arbitrary band filling in one, two and three dimensions as well as for $d = \infty$, using the Kotliar–Ruckenstein slave-boson mean-field approach. We have also demonstrated its equivalence to the explicitly spin- and charge-rotation-invariant method at the mean-field level. Due to the attraction–repulsion transformation, the results are also applicable to the half-filled repulsive Hubbard model. The attractive Hubbard model is one of the simplest for displaying a crossover from BCS to Bose-type superconductivity in the s-wave channel. Our results for superfluid characteristics substantiate and give further insight into the nature of the crossover from BCS-like to local pair (composite-boson) superconductivity.

The picture of smooth crossover from weak to strong coupling, obtained earlier within the broken-symmetry HFA [2] and the HFA–RPA (random-phase approximation) method for collective modes [4, 27, 25], at $T = 0$, is confirmed.

For the range of U-values and lattice structures considered, the calculated energy gap clearly indicates the advantage of the SBMFA over the HFA, especially as regards quantitative results. The energy gap agrees with the HFA only in the small-density limit. A comparison with the exact results in one dimension shows that the SBMFA introduces important corrections but still produces results quite far from the exact ones.

We have also examined the influence of the lattice dimensionality on the thermodynamic and electromagnetic properties of the model. We noted that there are two sets of units, the hopping integral t and the half-bandwidth D, which yield opposite behaviour of the model: if a parameter grows with the dimensionality, expressed in terms of one unit, it decreases when expressed in terms of the other. In t-units, the value of U/t for which the minimum of the band-narrowing factor and the maximum of the condensation energy occur, the absolute value of the condensation energy and the Ginzburg–Landau correlation length grow with increasing dimensionality. The ratio of the slave-boson energy gap to the Hartree–Fock energy gap and the London penetration depth λ decrease with growing dimensionality. In D-units, the behaviour is the opposite: whatever grows in t-units diminishes in D-units; what becomes smaller in t-units becomes larger in D-units. An interesting property is exhibited by the ratio of the SBMFA energy gap to the HFA energy gap at half-filling. In the weak-coupling limit the smallest value of the ratio is for $d = 1$; it is larger for $d = 3$ and largest for $d = 2$, irrespective of the units. This feature is related to the van Hove singularity for $d = 2$. For large U, the sequence depends on the dimensionality and the unit applied.

Another interesting feature connected with van Hove singularity was observed in the irregular behaviour of the band-narrowing factor q for the two-dimensional square lattice and the bcc lattice. This irregularity does not appear in the behaviour of the other quantities; it is concealed by the mean-field approximation.

The difference between the value of a given quantity calculated in the SBMFA method and the same quantity calculated in the HFA usually diminishes with growing $|U|$. One exception is provided by the Ginzburg–Landau correlation length, which turns out to measure the correlations among pairs. In the HFA the Ginzburg–Landau correlation length and the pair radius tend to 0 in the large-U limit, unlike the Ginzburg–Landau correlation length calculated in the SBMFA, which tends to a finite value. This is the case where the use of the SBMFA introduces qualitative changes.

Application of the SBMFA enables us to calculate the condensation energy, which is incorrectly overestimated in the HFA. We have found that, although the condensation energy is only a qualitative approximation to the critical temperature in all dimensions, we can obtain reasonable Uemura-type plots. We have also shown that T_c versus $1/\lambda^2$ and the ratio of the energy gap to the critical temperature exhibit scaling properties.

Our results for the case of infinite dimensions have shown that they are very good approximations to the ones for three dimensions, except for the energy gap, which for strong coupling is well approximated in the range of densities $n \gtrsim 0.5$. There will be no bound state in the empty-lattice limit for $d = \infty$, due to the infinite bandwidth for that case. Because the calculations based on a Gutzwiller wave function with and without Gutzwiller approximation using the SBMFA yield the same results for $d = \infty$ [26], we believe that this method becomes more accurate in high dimensions.

The SBMFA and HFA results presented confirm the smooth evolution of the electromagnetic properties and energy gap as well as the condensation energy from weak to strong coupling at $T = 0$, for all lattice dimensionalities and band fillings. Some quantities like the London penetration depth and the energy of the superconducting ground state are very close to the ones calculated in the HF approximation for all coupling strengths. Other quantities, like the energy of the normal state, the thermodynamic critical field and the Ginzburg–Landau correlation length agree with the HFA results only in the weak-coupling limit. This is due to the overestimation of the condensation energy by the HFA beyond the weak-coupling limit. The SBMFA yields reliable results in the intermediate- and strong-coupling regions which agree with perturbational treatments in the strong-coupling limit.

The approach presented, which is of mean-field type and does not include fluctuations of bosonic fields, can be extended in several ways. One is to consider inhomogeneous SB solutions, which could lead to non-linear, localized pairing bag excitations in a 2D lattice [28]. Second, it is of interest to examine fluctuation effects beyond the SBMFA, which can be especially relevant for finite-temperature crossover [19, 29]. This problem however awaits further studies.

Acknowledgments

This paper was supported by the State Committee for Scientific Research (KBN Poland): Projects No 2 PO3B 056 14 and No 2 PO3 B 104 11. We wish to thank B Bułka, S Robaszkiewicz and M Nogala for useful comments and discussion.

Appendix

Here we derive the free energy of the superconducting state in the SBMFA directly from the negative-U model, without resorting to the attraction–repulsion transformation. In this way we prove the equivalence of the approaches starting from the negative-U and from the positive-U Hubbard model.

We start from the negative-U Hubbard model, with the pairing field $\lambda^{(S)}$ added:

$$H = -t \sum_{i,j,\sigma} c^{\dagger}_{i\sigma} c_{j\sigma} - U \sum_{i} n_{i\uparrow} n_{i\downarrow} - \mu \sum_{i,\sigma} n_{i\sigma} + \frac{\lambda^{(S)}}{2} \sum_{i} \left(c^{\dagger}_{i\uparrow} c^{\dagger}_{i\downarrow} + c_{i\downarrow} c_{i\uparrow} - X \right) \tag{A1}$$

where $X = 2x_0$ is defined in equation (27). We apply the following canonical trans-

formation:

$$\begin{pmatrix} c_{i\uparrow} \\ c_{i\downarrow}^{\dagger} \end{pmatrix} = \begin{pmatrix} \cos\phi_i & \sin\phi_i \\ -\sin\phi_i & \cos\phi_i \end{pmatrix} \begin{pmatrix} c'_{i\uparrow} \\ c'^{\dagger}_{i\downarrow} \end{pmatrix} \tag{A2}$$

which corresponds to rotation in the space of charge operators ρ:

$$\rho_{ix} = (\rho_i^{\dagger} + \rho_i^{-})/2 \qquad \rho_{iy} = (\rho_i^{\dagger} - \rho_i^{-})/2\mathrm{i} \qquad \rho_{iz} = (n_{i\uparrow} + n_{i\downarrow} - 1)/2$$
$$\rho_i^{\dagger} = c_{i\uparrow}^{\dagger} c_{i\downarrow}^{\dagger} \qquad \rho_i^{-} = c_{i\downarrow} c_{i\uparrow}$$

with the same rotation matrix as in equation (7) and $\theta_i = 2\phi_i$. Let us note that

$$X = \langle \rho_i^{\dagger} \rangle + \langle \rho_i^{-} \rangle = (2/N) \sum_i \langle \rho_{ix} \rangle.$$

After this transformation, introducing the slave-boson operators, the saddle-point approximation for the Bose fields and transformation to the reciprocal space, we obtain (omitting the primes)

$$\begin{aligned} \mathcal{H} = \sum_{k\sigma} \Big[q\cos\theta\varepsilon_k - \frac{1}{2}(h\cos\theta + \lambda^{(S)}\sin\theta - U) - \lambda^{(2)} \Big] f_{k\sigma}^{\dagger} f_{k\sigma} \\ + \sum_k \Big[q\sin\theta\varepsilon_k + \frac{g}{2}(\lambda^{(S)}\cos\theta - h\sin\theta) \Big] (f_{k\uparrow}^{\dagger} f_{-k\downarrow}^{\dagger} + \mathrm{HC}) \\ + N \Big[-Ud^2 + \frac{h}{2}(\cos\theta - 1) + \frac{\lambda^{(S)}}{2}(\sin\theta - X) + 2\lambda^{(2)}(p^2 + d^2) \Big] \end{aligned} \tag{A3}$$

where $h \equiv 2\mu + U$; q is given by equation (11) and g by

$$g = \left\langle \frac{1}{\sqrt{1 - p_{i\sigma}^{\dagger} p_{i\sigma} - d_i^{\dagger} d_i}} e_i^{\dagger} d_i \frac{1}{\sqrt{1 - e_i^{\dagger} e_i - p_{i\bar{\sigma}}^{\dagger} p_{i\bar{\sigma}}}} \right\rangle \tag{A4}$$

with normalizing factors introduced like in equations (9) and (10). Next, we introduce the new variables

$$\frac{\bar{h}}{2} = \frac{h}{2} - \left(\frac{U}{2} - \lambda^{(2)} \right) \cos\theta \qquad \frac{\bar{\lambda}^{(S)}}{2} = \frac{\lambda^{(S)}}{2} - \left(\frac{U}{2} - \lambda^{(2)} \right) \sin\theta \tag{A5}$$

which make the Hamiltonian more symmetric and we diagonalize it by applying the Bogolyubov transformation. Taking into account the following relations:

$$\langle \rho'_z \rangle = \langle (n'_{i\uparrow} + n'_{i\downarrow} - 1)/2 \rangle = (2p^2 + 2d^2 - 1)/2 = p^2 + d^2 - 1/2 \tag{A6}$$

with $\langle \rho_x \rangle = -\langle \rho'_z \rangle \sin\theta$ and $\langle \rho_z \rangle = \langle \rho'_z \rangle \cos\theta$, we finally get the free energy of the superconducting state in the form

$$F = -\frac{2}{\beta N} \sum_k \ln[2\cosh(\beta E_k/2)] + Up^2 - \bar{\lambda}^{(S)} X/2 + \bar{h}(n-1)/2 - \frac{U}{2} n \tag{A7}$$

where

$$E_k = \sqrt{ \left[q\cos\theta\varepsilon_k - \frac{1}{2}(\bar{h}\cos\theta + \bar{\lambda}^{(S)}\sin\theta) \right]^2 + \left[q\sin\theta\varepsilon_k - \frac{g}{2}(\bar{h}\sin\theta - \bar{\lambda}^{(S)}\cos\theta) \right]^2 }. \tag{A8}$$

The slave-boson band-narrowing factors read

$$q = \frac{4p^2\big(1 - 2p^2 + \sqrt{(1-2p^2)^2 - m^2}\big)}{1 - m^2} \qquad g = \frac{2\sqrt{(1-2p^2)^2 - m^2}}{1 - m^2} \tag{A9}$$

where

$$m^2 = \langle (2\rho_z')^2 \rangle = \langle 4(\rho_x^2 + \rho_z^2) \rangle = (n-1)^2 + X^2.$$

When we replace p by d, X by $-m_x$ and $n-1$ by m_z, equations (A7)–(A9) reduce to equations (17)–(19), so we obtain the same results as in reference [10], where they were derived for the repulsive Hubbard model on a bipartite lattice for the half-filled band in a magnetic field. We notice that the formulation of the SBMFA given in this appendix applies to non-bipartite lattices as well.

References

[1] Lieb E H and Wu F Y 1968 *Phys. Rev. Lett.* **20** 1445
[2] Micnas R, Ranninger J and Robaszkiewicz S 1990 *Rev. Mod. Phys.* **62** 113 and references therein
[3] Randeria M 1995 *Bose–Einstein Condensation* ed A Griffin, D Snoke and S Stringari (Cambridge: Cambridge University Press) p 355
[4] Micnas R and Kostyrko T 1996 *Recent Progress in High Temperature Superconductivity (Springer Lecture Notes in Physics 475)* (Berlin: Springer) p 221
[5] Kotliar G and Ruckenstein A E 1986 *Phys. Rev. Lett.* **57** 1362
[6] Metzner W and Vollhardt D 1989 *Phys. Rev. Lett.* **62** 324
[7] Uemura Y J *et al* 1989 *Phys. Rev. Lett.* **62** 2317
Uemura Y J *et al* 1991 *Phys. Rev. Lett.* **66** 2665
Uemura Y J 1997 *Physica* C **282–287** 194
[8] Micnas R and Robaszkiewicz S 1997 *High-T_c Superconductivity 1996: Ten Years after the Discovery (NATO ASI Series E, vol 343)* ed E Kaldis, E Liarokapis and K A Müller (Dordrecht: Kluwer Academic) p 31 and references therein
[9] Denteneer P J H 1996 *Phys. Rev.* B **53** 9764
[10] Sofo J O and Balseiro C A 1992 *Phys. Rev.* B **45** 377
[11] Bułka B R and Robaszkiewicz S 1996 *Phys. Rev.* B **54** 13 138
Bułka B R 1993 *Phys. Status Solidi* b **180** 401
[12] Frésard R and Wölfle P 1992 *Int. J. Mod. Phys.* B **6** 685
[13] Robaszkiewicz S, Micnas R and Chao K A 1981 *Phys. Rev.* B **24** 4018
[14] Fetter A L and Walecka J D 1971 *Quantum Theory of Many-Particle Systems* (New York: McGraw-Hill)
[15] Jelitto R J 1969 *J. Phys. Chem. Solids* **30** 609
[16] Marsiglio F 1997 *Phys. Rev.* B **55** 575
[17] Carmelo J and Micnas R 1990 *J. Phys.: Condens. Matter* **2** 6981
[18] Denteneer P J H, An Guozhong and van Leeuven J M J 1993 *Phys. Rev.* B **47** 6256
[19] Hasegawa H 1989 *J. Phys.: Condens. Matter* **1** 9325
[20] Pan K and Wang Y 1997 *Phys. Rev.* B **55** 2981
[21] Jarrell M 1992 *Phys. Rev. Lett.* **69** 168
[22] Czart W, Kostyrko T and Robaszkiewicz S 1996 *Physica* C **272** 51
[23] Denteneer P J H 1994 *Phys. Rev.* B **49** 6364
[24] See, for example,
Pistolesi F and Strinati G 1996 *Phys. Rev.* B **53** 15 168
[25] Belikhir L and Randeria M 1994 *Phys. Rev.* B **49** 6829
[26] van Dongen P G J and Vollhardt D 1990 *Phys. Rev. Lett.* **65** 1663
Metzner W and Vollhardt D 1987 *Phys. Rev. Lett.* **59** 121
[27] Kostyrko T and Micnas R 1992 *Phys. Rev.* B **46** 11 025
[28] Bishop A R, Lomdahl P S, Schrieffer J R and Trugmann S A 1988 *Phys. Rev. Lett.* **61** 2709
[29] Gebhard F 1997 *The Mott Metal–Insulator Transition: Models and Methods (Springer Tracts in Modern Physics 137)* (Berlin: Springer)